Iranian Journal of Physics Research, Vol. 21, No. 3, 2021

Study of interaction between acoustic-Alfven waves in solar magnetic flux tubes

Z Fazel
Astrophysics Department, Physics Faculty, University of Tabriz, Tabriz, Iran

E-mail: z_fazel@tabrizu.ac.ir

(Received 16 September 2020 ; in final form 11 May 2021)

Abstract
Solar acoustic oscillations are actually the same 5 minute oscillations that appear in the photosphere. These oscillations appear to be unable to penetrate into the solar corona due to the acoustic cut off of stratified atmosphere and the sharp temperature gradient in the transition region. The 5 minute acoustic oscillations may resonantly convert into Alfven waves in the $\beta \approx 1$ region of the solar atmosphere. By perturbing the equilibrium state of the magnetised plasma, we showed that the acoustic and Alfven waves can interact through the nonlinear terms of the ideal MHD equations. We found that Alfven waves with twice the period of acoustic waves may propagate to upper layers when the speeds of sound and Alfven waves are equal, $c_s \approx v_A$. This condition is obtained when, $\varpi_A = \frac{1}{2}\varpi_s$.

Keywords: solar magnetic flux tubes, Alfven waves, acoustic oscillations, resonant conversion

1. Introduction

The heating mechanisms of the solar upper atmospheric layers (the chromosphere and corona) are one of the most important fields of research in solar physics. Helioseismology can demonstrate the behavior of solar phenomena by using the observed oscillations [1, 2]. A general method for heating of the solar upper atmosphere is the damping of magnetohydrodynamics (MHD) waves. When MHD waves interact with plasma inhomogeneities (e.g. density, velocity and magnetic field), a number of physical events are generated such as wave dispersion, phase mixing [3, 4], mode coupling [5, 6] and resonant absorption [7, 8, 9].

Safari et al. (2006) [10] studied the resonance absorption of MHD waves in magnetized flux tubes with a radial density inhomogeneity. The ohmic and viscous dissipations were assumed in a thin boundary layer. They obtained an analytical dispersion relation and solved it numerically. They have shown that as longitudinal wave number increases, the maximum amplitude of the body eigenmodes shifts away from the resonant layer and causes a decrease in damping rates.

It is usually considered that solar 5-min acoustic oscillations in photosphere cannot make a way into the upper layers because of the cutoff of stratified atmosphere and of the sharp temperature gradient in the transition layer. However, 5-min oscillations are observed in the solar corona by SOHO and TRACE space satellites [11]. De Pontieu et al. (2005) [12] have studied about the penetration of photospheric waves into the corona by the inclined magnetic fields. Bogdan et al. (2003) [13] have investigated the importance of $\beta \sim 1$ region in the solar atmosphere by two dimensional numerical simulations. They showed that the mode coupling of MHD waves takes place at this region. Muglach et al. (2005) [14] have presented from observations that transformation of the compressible wave energy to incompressible waves are possible at this $\beta \sim 1$ region.

Shergelashvili et al. (2005) [15] have investigated about "swing absorption" of fast magnetosonic waves in inhomogeneous media. They showed that the fast magnetosonic waves propagating across an applied non-uniform magnetic field can parametrically amplify the Alfven waves propagating along the field through the periodical variation of the Alfven speed. The resonant Alfven waves have half the frequency and the perpendicular velocity polarization of the fast waves. The wavelengths of the resonant waves have different values across the magnetic field, due to the

inhomogeneity in the Alfven speed. Kuridze et al. (2005) [16] have studied resonant conversion of standing acoustic oscillations into Alfven waves in the $\beta \sim 1$ region of the solar atmosphere. They found that an acoustic oscillation is non-linearly coupled to the Alfven wave with double the wavelength and period when $c_s \approx v_A$. The region of the solar atmosphere where this equality takes place are called a swing layer.

From observational view, Ganjali et al. (2018) [17] have analyzed the transvers oscillations of the coronal loop observed from SDO/AIA. They concluded that the damping of transvers oscillations of the coronal loop in is the strong damping regime in which the resonance absorption would be a well suitable candidate for the loop damping mechanism.

In this paper, we study the resonant conversion of the acoustic oscillations to Alfven waves in a typical magnetic flux tube by numerical simulation. Sections 2, 3 and 4 give the basic equations and theoretical model. We consider the ideal MHD equations without dissipation terms, but for coupling modes we apply non-linear terms of MHD equations. In section 5, numerical results are presented, and the conclusion is followed in section 6.

2. Theoretical modeling

We consider a solar flux tube in 2D x-z plane in the presence of steady flow and shear field. The mode conversion of photospheric acoustic oscillations into Alfven waves is studied at the solar chromosphere. For simplicity the stratification is neglected. By considering fluid motions in a magnetized region (with any dissipation process), the ideal MHD equations in the plasma dynamics are as follows:

$$\rho\frac{\partial\vec{V}}{\partial t}+\rho(\vec{V}.\nabla)\vec{V}=-\nabla p+\frac{1}{\mu_0}(\nabla\times\vec{B})\times\vec{B} \quad (1)$$

$$\frac{\partial\vec{B}}{\partial t}=\nabla\times(\vec{V}\times\vec{B}),\nabla.\vec{B}=0 \quad (2)$$

where V is the plasma velocity, B is the magnetic field, μ_0 is the vacuum permeability, ρ is the plasma density and $P=\frac{\rho RT}{\mu}$ is the pressure for perfect gas. μ is the mean molecular weight.

The equilibrium state

The velocity and magnetic fields are defined as follows:

$$\vec{V}=\vec{V}_0+\vec{v}$$
$$\vec{B}=\vec{B}_0+\vec{b} \quad (3)$$

where $\vec{V}_0=0$ and $\vec{B}_0=\exp(k_b(x-1))\hat{k}$ are the equilibrium velocity and magnetic fields of the plasma. The density and pressure are also assumed to have x dependence, they are expressed as $\rho_0(x)$ and $p_0(x)$, respectively. The equilibrium density profile is considered as:

$$\rho_0(x)=\rho_0\left[2+\tanh\left(\alpha(x-1)\right)\right]^{-2} \quad (4)$$

The magnetic field and pressure satisfy the transverse pressure balance condition:

$$\nabla(p_0(x)+\frac{{B_{0z}}^2(x)}{8\pi})=0 \quad (5)$$

where $p_0(x)=p_0(T_0,\rho_0(x))$. We are also considered plasma β as

$$\beta=\frac{8\pi p_0(x)}{{B_{0z}}^2(x)} \quad (6)$$

Perturbation equations

In order to make continuous displacements of the flux tube, a perturbation in the velocity and magnetic field is considered at the lower boundary of the tube. Vectors $\vec{v}$ and $\vec{b}$ in equation (3) are the perturbed velocity and magnetic field which are defined as $\vec{v}=(0,v_y,v_z)$ and $\vec{b}=(0,b_y,0)$, respectively. The wave propagation is considered along z-axis. Only sound and Alfven waves appear, the velocity component of Alfven wave is polarized along y-axis and the velocity component of sound wave is polarized along z-axis. We study the weakly non-linear regime. In other words, the amplitudes of the waves are considered to be large enough to produce variations of the environment parameters (can be seen by propagating Alfven modes), but too small to affect the Alfven waves themselves. From analytical work [16], when wave numbers satisfy the condition $k_S=2k_A$, the waves can interact via the non-linear terms remained in the equations.

Here, we first introduce the perturbed MHD equations by considering of some non-linear terms, and then by numerical solving of the equations we expect to see the condition as mentioned above. In order to see the variations of the perturbed velocity and magnetic field, the ideal dimensionless MHD equations with the considered assumptions are as follows:

$$\frac{\partial v_y}{\partial t}=\frac{B_{0z}(x)}{\rho_0+\rho_1}\frac{\partial b_y}{\partial z}-v_z\frac{\partial v_y}{\partial z} \quad (7)$$

$$\frac{\partial v_z}{\partial t}=-\frac{b_y}{\rho_0+\rho_1}\frac{\partial b_y}{\partial z}-v_z\frac{\partial v_z}{\partial z}-\frac{1}{\rho_0+\rho_1}\frac{\partial p}{\partial z} \quad (8)$$

$$\frac{\partial b_y}{\partial t}=B_{0z}(x)\frac{\partial v_y}{\partial z} \quad (9)$$

where density, velocity, magnetic field, time and space coordinates are normalized to ρ, V_{A0}, B_0, τ, and a (the typical flux tube radius), respectively. Eqs. (7-9) should be solved numerically under following perturbations and boundary conditions:

$$v_y(x,z,t=0)=A_v\sin(k_A(z-1))\sin(kx) \quad (10)$$

$$v_z(x,z,t=0)=A_v\cos(k_s(z-1))\sin(kx) \quad (11)$$

$$b_y(x,z,t=0)=A_b\sin(k_A(z-1))\cos(kx) \quad (12)$$

$$\rho(x,z,t=0)=A_\rho\cos(k_s(z-1))\sin(kx) \quad (13)$$

where A_v, A_b, A_ρ are the small amplitudes of the perturbed velocity, magnetic field and density respectively. The k_A and k_S are the Alfven and acoustic wave numbers. The pressure profile is the same as density one. The boundary conditions are defined as:

$$v_y(x=0,z,t)=v_y(x=4,z,t)=0,\leq$$
$$v_y(x,z=0,t)=v_y(x,z=20,t)=0,$$

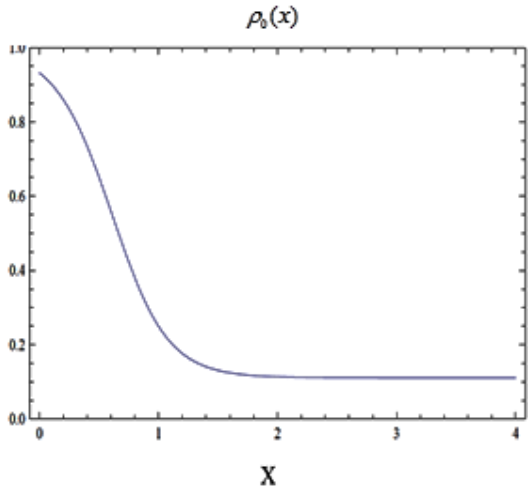

Fig 1. The profile of the equilibrium density plotted with respect to dimensionless x.

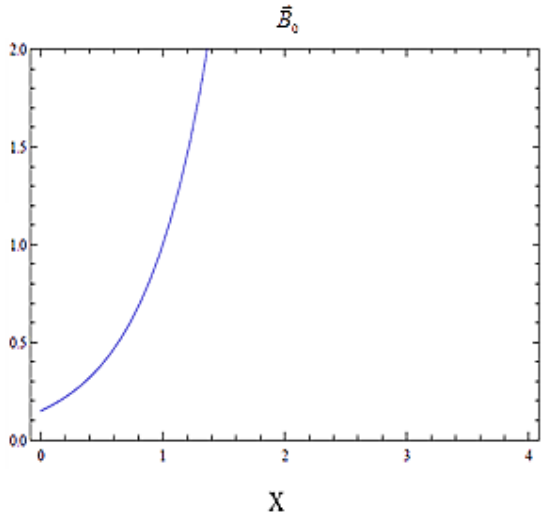

Fig 2. The profile of the equilibrium magnetic field plotted with respect to dimensionless x.

$$b_y(x=0,z,t)=b_y(x=4,z,t)=0,$$
$$b_y(x,z=0,t)=b_y(x,z=20,t)=0.$$

With the use of equation (4) we obtain the mass density profile which show the variation of the initial plasma density in the flux tube (Fig 1).

Figure 2 shows the variation of equilibrium magnetic field in the flux tube by using equation $\vec{B}_0=\exp(k_b(x-1))\hat{k}$.

3. Numerical results

To solve the coupled Eqs. (7-9) numerically, the finite difference and the Fourth-Order Runge-Kutta methods are used to take the space and time derivatives, respectively. The implemented numerical scheme relies on the forward finite difference method to take the first spatial derivatives with a truncation error of (Δx), which is spatial resolution in the x direction. The order of approximation for the second spatial derivate in the finite difference method is $O((\Delta x)^2)$. On the other hand, the forth-order Runge-Kutta method takes the time derivatives into account.

We set the number of mesh-grid points as 256×256. In addition, the time step is chosen as 0.01, and the system length in the x and z dimensions (simulation box sizes) are set to be (0, 4) and (0, 20). The parameters in a flux tube (for example in a spicule) are as follows:
a= 250 km (typical spicule radius), L= 5000 km (Spicule length), d= 0.5 Mm (the width of initial pulse), n_e= 11.5×10^{16} m^{-3}, B_0= 1.2×10^{-3} Tesla, T_0= 14000 K, R= 8300 m^2/sK (universal gas constant), V_{A0}= 50 km/s, μ= 0.6, ρ_0= 1.9×10^{-10} kg/m^3, p_0= 3.7×10^{-2} N/m^2, μ_0= $4\pi\times10^{-7}$ Tesla m/A, x_0= 1000 km, z_0= 125 km, A_v= 5 km/s, k_a= π/16, and k_s= π/8 (dimensionless wavenumber normalized to a), α= 2, β=1 and τ= 4 s.

Figure 3 illustrates the 3D plots of the z-component of the perturbed velocity with respect to x, z for t= 25τ s and t= 125τ s. In these plots, the increment of the velocity amplitude is seen with respect both x- and z-axes. The initial pulse amplitude is 5 km/s and is located in x=500 km and z=125 km. It shows that the initially localized pulse, which is launched in the lower chromosphere, propagates upward.
Similar to figure 3, in figure 4 the same plot of the perturbed z-component velocity with respect to x,

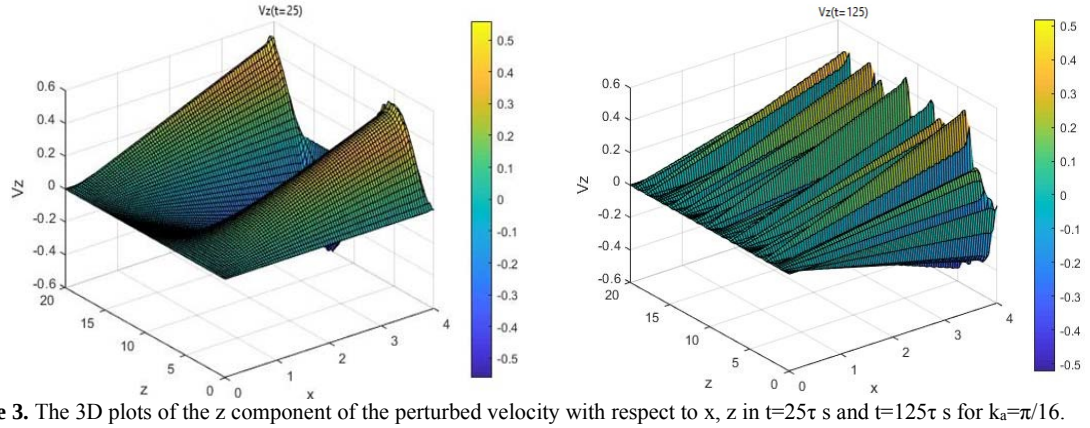

Figure 3. The 3D plots of the z component of the perturbed velocity with respect to x, z in t=25τ s and t=125τ s for $k_a=\pi/16$.

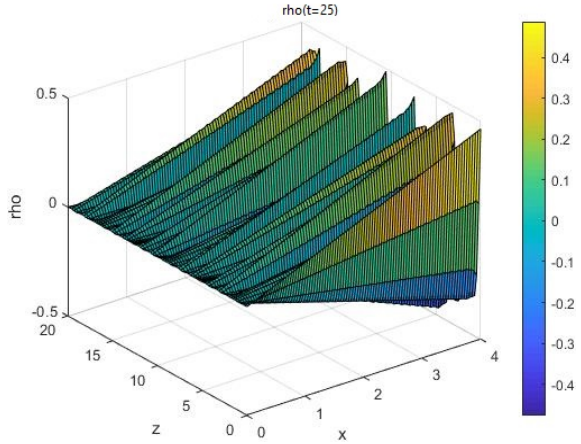

Figure 4. The 3D plot of the perturbed density with respect to x, z in t=25τ s and t=125τ s for $k_a=\pi/16$.

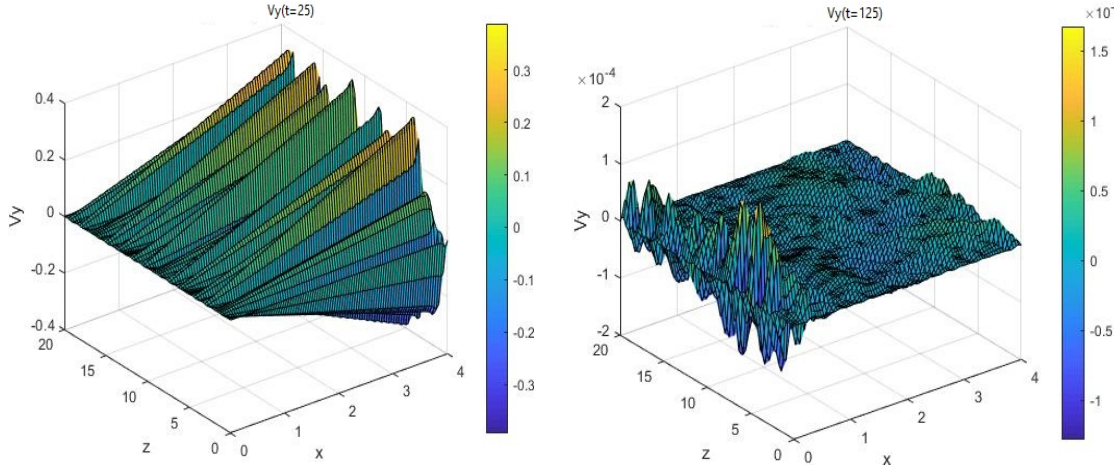

Figure 5. The 3D plots of the transversal component of the perturbed velocity with respect to x, z in t=25τ s and t=125τ s for $k_a=\pi/16$.

z at t= 25τ s is presented. Obviously a similar pattern of upward propagation of the initially localized pulse is repeated here.

Figures 5 and 6 illustrate the 3D plots of the y-component of the perturbed velocity and magnetic field with respect to x, z for t= 25τ s and t= 125τ s. The initial pulse is located in x=1000 km and z=500 km. In these figures, the behavior of the y-component of the velocity and magnetic field are seen to be the same.

Figure 7 shows the variations of the perturbed density and the z-component of velocity with time (dimensionless). In these plots, the propagation of the acoustic oscillations are seen with time. The period of these oscillations is seen about $20\tau\, s$, and an increment of the amplitude takes place around $t=190\tau\, s$. According to equation (8), we showed that the z-component of the velocity is coupled with the y-component of the magnetic field through the non-linear

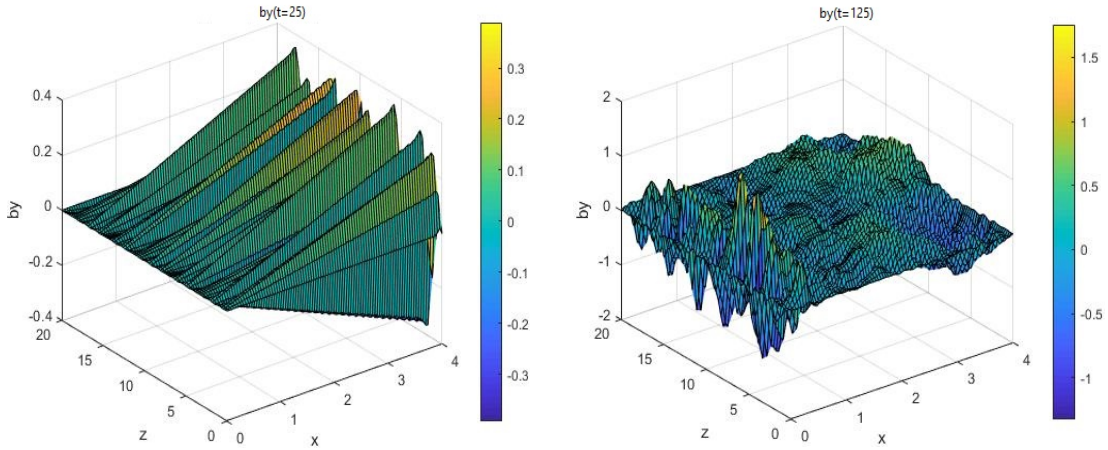

Figure 6. The 3D plots of the z component of the perturbed magnetic field with respect to x, z in t=25τ s and t=125τ s for $k_a=\pi/16$.

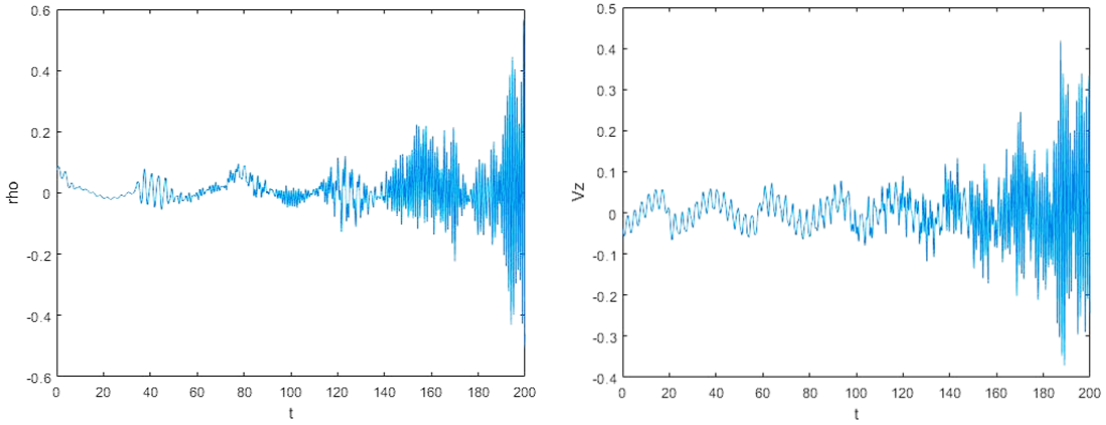

Figure 7. Temporal variations of the perturbed density and velocity (dimensionless).

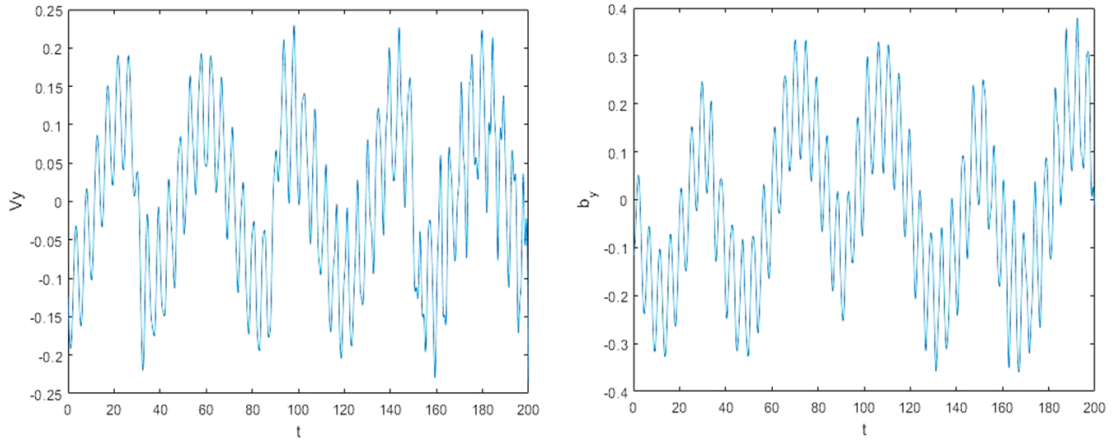

Figure 8. Temporal variations of the perturbed velocity and magnetic field (dimensionless).

terms. The acoustic and Alfven waves would interact through these nonlinear terms when $k_S = 2k_A$.

Figure 8 demonstrates the temporal variations of the y-component of the perturbed velocity and magnetic field (dimensionless). According to the equation (9), the Alfven wave propagates in direction of the y axis with period $\tau_A = 40\tau\, s = 2.6\, min$. This period is in good agreement with the life time of a typical spicule (5-15 min) in the solar chromosphere [18].

By comparing of two obtained periods above, Alfven waves propagate with twice the period of acoustic oscillations. Analytical solution of the wave equations showed that the resonant solution will occur when $\omega_A = v_A k_A = \frac{\omega_S}{2}$ (ω_A is the frequency of Alfven waves) [16]. We also obtained from numerical computations that the resonance takes place when $k_A = \frac{k_S}{2}$ (in other words, $\omega_A = \frac{\omega_S}{2}$) satisfying $c_s \approx v_A$.

4. Conclusion

The interaction between the MHD waves may take place either because of inhomogeneity or nonlinearity. The nonlinearity interrelation between waves is well grow as resonant triplets [8]. Other methods of wave damping are including phase mixing and resonant absorption which are related to the inhomogeneity of the plasma. In this work, we have considered the ideal MHD equations with non-linear interaction between two waves in a medium with a steady background flow and non-uniform magnetic field. The acoustic oscillations (5-min oscillations) can be resonantly converted into Alfven waves in the thin magnetic tubes. This mode conversion takes place in a region of the solar atmosphere where $c_s \approx v_A$ or $\beta \sim 1$ (this region is called swing layer [16]). In our numerical simulation, we have considered the perturbations in the density, velocity and magnetic field of the plasma as a function of wave number. We were looking for a condition on these wave numbers to obtain the resonance layer. In plots of figure 7, an increase of the amplitude of the oscillation is observed in $t = 190\,\tau\, s$ (this is in good agreement with the life time of a typical chromospheric spicule) for $k_A \sim \frac{1}{2} k_S$. The enhanced Alfven waves may then propagate through the upper atmosphere and transfer their energy into corona.

References

1. T V Zaqarashvili, E Khutsishvili, V Kukhianidze and G Ramishvili, *Astron. & Astrophys*., **474** (2007) 627
2. M Aschwanden, *NATO Science Ser*. (K;uwer Academic Publications) 2003.
3. J Heyvaerts, and E R Priest, *Astron. & Astrophys*., **117** (1983) 220.
4. V M Nakariakov, B Roberts, and K Murawski, *Sol. Phys.*, **175** (1997) 93.
5. D J Pascoe, A W Hood, I De Moortel, and A N Wright, *Astron. & Astrophys*., **539** (2012) 37.
6. Z Fazel, *Res. in Astron. & Astrophys.*, **16**, 1 (2016) 1.
7. J A Ionson, *Astrophys. J.,* **226** (1978) 650.
8. J V Hollweg, *Astrophys. J.,* **317** (1987) 514.
9. L Ofman, and J M Davila, *J. Geophys. Res*., **100** (1995) 23427.
10. H Safari, S Nasiri, K Karami, and Y Sobuti, *Astron. & Astrophys.,* **448** (2006) 375.
11. I De Moortel, J Ireland, A W Hood and R W Walsh, *Astron. & Astrophys.,* **387** (2002) 13.
12. B De Pontieu , R Erdelyi and I De Moortel, *Astrophys. J.,* **624** (2005) 61.
13. T J Bogdan, M Hansteen, V Carlsson, et al., *Astrophys. J.*, **599** (2003) 626.
14. K Muglach, A Hofmann and J Staude, *Astron. & Astrophys.,* **437** (2005) 1055.
15. B. M Shergelashvili, T.V. Zaqarashvili, S. Poedts and B. Roberts, *Astron. & Astrophys.*, **429** (2005) 767.
16. D Kuridze, T V Zaqarashvili and B Roberts, *ESA SP-596,* (2005).
17. J Ganjali, N Farhang, SH Esmaeili, M Javaherian, and H Safari, *Iranian J. of Astron. & Astrophys.*, **5**, No 2 (2018) 75.
18. 18. H Ebadi, T V Zaqarshvili, and I Zhelyazkov, *Astrophys. Space Sci.* **337** (2012a) 33.